ELSEVIER

Journal of Fluids and Structures 24 (2008) 757–777

JOURNAL OF FLUIDS AND STRUCTURES

www.elsevier.com/locate/jfs

Nonlinear aeroelastic behavior of an oscillating airfoil during stall-induced vibration

S. Sarkar[a,*], H. Bijl[b]

[a]*Department of Aerospace Engineering, Indian Institute of Technology Madras, Chennai 600036, India*
[b]*Faculty of Aerospace Engineering, Delft University of Technology, Kluyverweg 1, 2629 HS Delft, The Netherlands*

Received 20 February 2006; accepted 6 November 2007
Available online 28 January 2008

Abstract

In this paper, nonlinear aeroelastic behavior of a two-dimensional symmetric rotor blade in the dynamic stall regime is investigated. Two different oscillation models have been considered here: pitching oscillation and flap–edgewise oscillation. Stall aeroelastic instability in such systems can potentially lead to structural damage. Hence it is an important design concern, especially for wind turbines and helicopter rotors, where such modes of oscillation are likely to take place. Most previous analyses of such dynamical systems are not exhaustive. System parameters like structural nonlinearity or initial conditions have not been studied which could play a significant role on the overall dynamics. In the present paper, a parametric study on the aeroelastic instability and the nonlinear dynamical behavior of the system has been performed. Emphasis is given on the effect of structural nonlinearity and initial conditions. The aerodynamic loads in the dynamic stall regime have been computed using the Onera model. The qualitative influence of the system parameters is different in the two systems studied. The effect of structural nonlinearity on the bifurcation pattern of the system response is significant in the case of pitching oscillation. The initial condition plays an important role on the aeroelastic stability as well as on the bifurcation pattern in both the systems. In the forced response study, interesting dynamical behavior, like period-3 response, has been observed in the pitching oscillation case. On the other hand, for the flap–edgewise oscillation case, super-harmonic and quasi-harmonic response have been found.

Keywords: Dynamic stall; Stall flutter; Pitching oscillation; Flap–edgewise oscillation

1. Introduction

There are many instances where stall-induced oscillation leads to structural failure. Instances of longitudinal crack formation in modern wind turbines is reported by Chaviaropoulos (1999) which resulted from severe edgewise vibration. This has occurred during the dynamic stall process in modern stall-regulated turbines. In general, an airfoil oscillates along the pitch degree-of-freedom during stall flutter. The flow-field during the dynamic stall process is largely separated and viscous effects are important. The physical process involves growth and evolution of leading edge vortex structures and their subsequent shedding from the body into the near wake. This largely controls the aerodynamic loads on the airfoil. The flow field involves flow transition and large turbulent regions as well. All these effects make the

*Corresponding author.
E-mail address: sunetra.sarkar@gmail.com (S. Sarkar).

0889-9746/$ - see front matter © 2008 Elsevier Ltd. All rights reserved.
doi:10.1016/j.jfluidstructs.2007.11.004

aerodynamic load prediction during a stall flutter problem much more involved than its traditional bending-torsion counterpart. In the present study, we investigate a stall flutter problem along the pitch-wise and in the flap–edgewise directions separately. A parametric study has been performed in order to understand the influence of system parameters on the nonlinear dynamics and aeroelastic stability. This study is relevant toward the aeroelastic design of systems where large angles of attack are likely to be encountered, such as in wind turbines.

The main objective of any computational aeroelastic analysis is to define the instability boundary and identifying the system parameters affecting it. Nonlinearity could play an important role, for it could influence the aeroelastic stability and could lead to bifurcations and chaos in the response. Dunn and Dugundji (1992) have presented an analysis and experimental validation of aeroelastic instabilities at the nonlinear dynamic stall regime for a cantilever plate-like wing structure. Tang and Dowell (1993a, b) have studied flutter and forced response of a helicopter rotor in the bending-torsion mode, using a nonlinear aerodynamic model and considering geometric and free-play structural nonlinearities. They have also performed experimental studies and obtained a good match with the analytical results. The dynamic stall model used in the analysis is based on a semi-empirical technique called the Onera dynamic stall model. Lee et al. (1999) have presented a review of nonlinear aeroelastic studies focusing on the pitch–plunge oscillation of an airfoil. They have discussed problems with both structural and aerodynamic nonlinearities. Structural nonlinearities, in general, have been represented by the classical forms of cubic, free-play and hysteresis. Price and Fragiskatos (2000) have presented a nonlinear stall flutter analysis of a symmetric airfoil, using a nonlinear dynamic stall model by Beddoes–Leishman. However, they have not considered the effect of structural nonlinearity. Chaviaropoulos (1999) and Chaviaropoulos et al. (2003) have presented a study on stall-induced flap and edgewise oscillation in a stall-regulated rotor. Nonlinear aerodynamic loads in the dynamic stall regime have been calculated by a quasi-steady Onera model as well as Navier–Stokes solvers (Chaviaropoulos et al., 2003). Effects of structural nonlinearity have not been studied.

The present study considers stall flutter of an airfoil in two different structural models: a single-degree-of-freedom pitching oscillation and a two-degree-of-freedom flap–edgewise oscillation in the dynamic stall regime. The first model is the fundamental stall flutter model representing predominantly torsional oscillation. The second problem is reportedly encountered in stall-regulated rotors, where pitch-wise oscillation is restricted (Chaviaropoulos, 1999). Most earlier works with similar models have considered the effect of aerodynamic nonlinearity alone. The present work investigates the effect of structural nonlinearity as well. Moreover, previous analysis do not report the effect of initial conditions which has been addressed now. The influence of other system parameters has also been included which helps in a systematic understanding of the stall flutter phenomenon in the above aeroelastic models. The aerodynamic loads have been calculated by the semi-empirical Onera dynamic stall model; this model compares well with the experimental results and is computationally much more efficient than a Navier–Stokes solver.

Compared to Navier–Stokes solvers, semi-empirical dynamic stall models are much faster. Among them, the Onera model (Tran and Petot, 1981) and the Beddoes–Leishman model (Leishman and Beddoes, 1989) are quite commonly used (Petersen et al., 1998). The Beddoes–Leishman model describes the unsteady loads by an indicial method below the stall boundary, and above stall uses experimental data and a heuristic approach based on oscillating and ramping airfoil analysis (Leishman and Beddoes, 1989; Beedy et al., 2003). The Onera model was developed in the Office National d'Etudes et de Recherches Aérospatiales (ONERA) to compute the unsteady aerodynamic loads in the dynamic stall regime for a pitching airfoil (Tran and Petot, 1981) and was later extended for both pitch and plunge motions (Peters, 1985). The model is based on a semi-empirical approach. The aerodynamic loads are given in terms of differential equations, whose coefficients are determined empirically from experimental data by parametric fitting. The present study uses the Onera model; the parameters are obtained from previous literature (Dunn and Dugundji, 1992), in the Reynolds number and frequency range of our interest.

In the next section, a discussion on the Onera dynamic stall model is given. In Section 3, the equations of motion are derived for the two aeroelastic systems considered in this paper. In Section 4, a discussion of results is presented. And finally, in Section 5, a summary of the main observations from this work is given along with the conclusions.

2. Onera dynamic stall model

The physical process of dynamic stall refers to a complex dynamical phenomenon involving the development of leading and trailing edge vortex structures, their separation and shedding into the wake and mutual interactions. Vortex growth increases the aerodynamic loads beyond their stall boundary and shedding causes the decline. The loads are dependent on the frequency or the rate of airfoil movement. The Onera model is divided into two equations: for the inviscid part, and for the viscous part which becomes important above the stall angle of attack.

For details of the Onera model, Dunn and Dugundji (1992) and Tran and Petot (1981) can be referred to. Dunn and Dugundji (1992) compared Onera results with experiments for a NACA 0012 airfoil oscillating sinusoidally.

The comparisons were favorable; the overall shape of the aerodynamic load hysteresis curves was captured well. However, the high frequency components were not suitably captured and it was argued by Dunn and Dugundji (1992) that they do not play any significant role on the overall aeroelastic behavior of the system.

In the Onera model, the aerodynamic loads are given in terms of differential equations, for the inviscid and the viscous parts separately. The coefficients of the inviscid part, are obtained from steady state experimental results and are dependent on the airfoil profile. The viscous part uses parameters from unsteady experiments; the coefficient values, therefore, are dependent on dynamic parameters such as frequency.

The aerodynamic loads are given in terms of the following equations:

$$C_z = s_z\alpha' + k_{vz}\theta'' + C_{z1} + C_{z2}, \tag{1}$$

$$C'_{z1} + \lambda_z C_{z1} = \lambda_z(a_{oz}\alpha + \sigma_z\theta') + \alpha_z(a_{oz}\alpha' + \sigma_z\theta''), \tag{2}$$

$$C''_{z2} + 2dwC'_{z2} + w^2(1+d^2)C_{z2} = -w^2(1+d^2)(\Delta C_z|\alpha + e\Delta C'_z|\alpha). \tag{3}$$

Here, θ is the pitching angle and $\alpha = \theta - \dot{h}$ is the total angle of attack, where h refers to the flapping displacement. C_z is the general term for any one of the aerodynamic load coefficients C_L, C_D, C_M. The term C_{z1} is the inviscid circulatory part of the load and C_{z2} is the viscous part. s_z, k_{vz}, λ_z, α_z, a_{oz}, σ_z, d, w and e are the coefficients associated with the appropriate force coefficients, determined empirically by a parameter identification technique. The coefficients used in this study are taken from Dunn and Dugundji (1992) for a NACA 0012 airfoil.

The differential equation for each part has been modeled in such a way that the mathematical model resembles the complex physical process as closely as possible. The first-order inviscid equation, Eq. (2), uses a single lag term operating on the linear part of an airfoil's static force. It models the increase of the aerodynamic loads beyond the static stall angle. The viscous part, Eq. (3), takes care of the decrease of the loads during the dynamic stall hysteresis loop. ΔC_z in the viscous equation refers to the difference in the aerodynamic loads between the inviscid and the actual(viscous) value at any α greater than the static stall angle. Below the static stall angle, ΔC_z is zero. The differential equations of the Onera model are combined with the governing equations of the structural system to arrive at the equations of motion of the aeroelastic system. The system equations of motion are derived in the following section.

3. Equations of motion

To derive the equation of motion of a two-dimensional blade section, we consider a strip of unit span of a symmetric airfoil. A NACA 0012 profile has been selected. A schematic plot of the structure and its coordinate system is given in Fig. 1. Two oscillation cases have been considered: one is an airfoil oscillating in the pitch degree-of-freedom, the second is an airfoil oscillating in the directions of its flap and edge. The first case represents the classical stall flutter case of an airfoil which is predominantly a single-degree-of-freedom problem where the torsional motion of the blade

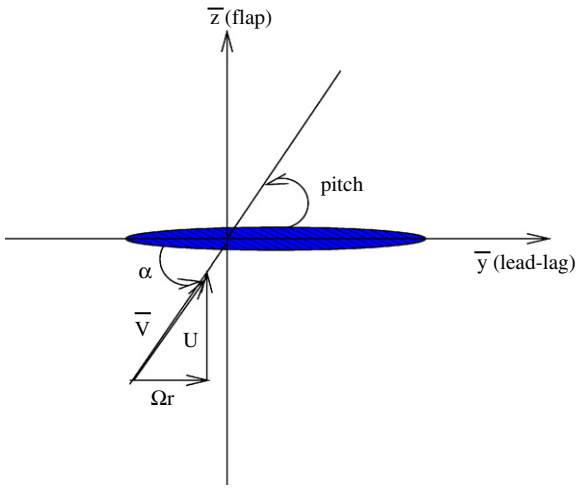

Fig. 1. Schematic plot of the airfoil coordinate system and oscillation degrees-of-freedom.

prevails. The second case is obtained in stall-regulated rotors showing sustained oscillation in the flap and edgewise directions.

3.1. Pitching oscillation

The equation of motion for the single-degree-of-freedom pitching oscillation is given as follows (Fung, 1955):

$$I_\alpha \ddot{\alpha} + I_\alpha \omega_\alpha^2 \alpha + K_{\mathrm{nl}} = M(t) + Q(t), \tag{4}$$

where I_α is the wing mass moment of inertia, α is the effective angle of attack, ω_α is the natural frequency of the pitch elastic mode and K_{nl} is a nonlinear stiffness term accounting for any structural nonlinearity present in the system. $M(t)$ is the time-dependent aerodynamic moment and $Q(t)$ is any applied external moment. A nondimensional form of the governing equation is often helpful in aeroelastic analysis to investigate the effect of system parameters. A nondimensional form of Eq. (4) is

$$\alpha'' + \alpha/(U^2) + \bar{K}_{\mathrm{nl}} = 2C_m/(\pi\mu r_\alpha^2) + F_0 \sin(k_1\tau), \tag{5}$$

where the prime denotes a derivative with respect to nondimensional time $\tau = t\bar{V}/b$, $\bar{V}$ is the relative wind velocity and b is the semi-chord of the profile. The aerodynamic moment coefficient C_m is calculated using the Onera dynamic stall model discussed in the previous section. U is the nondimensional airspeed defined as $U = \bar{V}/b\omega_\alpha$, μ and r_α are nondimensional structural parameters, $\mu = m/(\pi\rho b^2)$ is the mass ratio and $r_\alpha = I_\alpha/(mb^2)$ is the radius of gyration, where m is the mass per unit span. F_0 and $\bar{K}_{\mathrm{nl}}$ are nondimensional forcing amplitude and structural nonlinear stiffness, respectively; k_1 is the reduced frequency of oscillation. In the present study, a concentrated structural nonlinearity is incorporated in the form of a cubic stiffness $\bar{K}_{\mathrm{nl}} = K_{\mathrm{nl}1}\alpha^3$. This artifice has been used in the literature to model the stiffening spring behavior of a blade being twisted (Lee et al., 1999). Also, this is often a standard way to consider some control mechanisms that may be present in the structure (Alighanbari and Price, 1996; Tang and Dowell, 1993b).

3.2. Flap–edgewise oscillation

The equations of motion for the combined flap–edge flutter case for a rotating blade have been derived by Chaviaropoulos (1999). These equations are

$$\begin{bmatrix} 1 & 0 \\ 0 & 1 \end{bmatrix} \begin{Bmatrix} \ddot{\zeta} \\ \ddot{\beta} \end{Bmatrix} + \Omega \begin{bmatrix} 0 & 2\beta_0 \\ -2\beta_0 & 0 \end{bmatrix} \begin{Bmatrix} \dot{\zeta} \\ \dot{\beta} \end{Bmatrix} + \left(\begin{bmatrix} \omega_y^2 & 0 \\ 0 & \omega_z^2 \end{bmatrix} + \begin{bmatrix} 0 & 0 \\ 0 & \Omega^2 \end{bmatrix} \right) \begin{Bmatrix} \zeta \\ \beta \end{Bmatrix} = \frac{1}{2}\frac{\rho}{m}\bar{V}^2\frac{c}{r} \begin{Bmatrix} C_y \\ C_z \end{Bmatrix}, \tag{6}$$

where ζ and β are the small angular movements of the blade in the edge and flapwise directions, respectively, β_0 is the pre-cone angle of the blade and Ω is the rotational velocity. An extra stiffness term comes in the flap direction due to rotation of the blade. ρ is the constant density of the fluid, m is the blade mass per unit length of the blade and C_y, C_z are the aerodynamic load coefficients in the edge and flapwise directions, respectively. C_y, C_z are obtained from the lift and drag coefficients of the section by using a simple rotational transformation. Using a similar nondimensionalization as in Eq. (5), we obtain

$$\begin{bmatrix} 1 & 0 \\ 0 & 1 \end{bmatrix} \begin{Bmatrix} \bar{y}'' \\ \bar{z}'' \end{Bmatrix} + k^2 \begin{bmatrix} \bar{\omega}_y^2 & 0 \\ 0 & 1+\bar{\omega}_z^2 \end{bmatrix} \begin{Bmatrix} \bar{y} \\ \bar{z} \end{Bmatrix} = \frac{1}{2\pi\mu} \begin{Bmatrix} C_D\cos\alpha - C_L\sin\alpha \\ C_D\sin\alpha + C_L\cos\alpha \end{Bmatrix} + \begin{Bmatrix} 0 \\ \bar{F}_0\sin(k_1\tau) \end{Bmatrix}. \tag{7}$$

Here, $\bar{y} = \zeta r/b$ and $\bar{z} = \beta r/b$ are nondimensional edge and flapwise displacements, respectively; r is the radial distance of the blade section from rotor root; b is the semi-chord of the airfoil. Nondimensional stiffness terms are defined as $\bar{\omega}_y = \omega_y/\Omega$ and $\bar{\omega}_z = \omega_z/\Omega$. The rotor angular velocity is given in terms of the nondimensional term $k = \Omega b/\bar{V}$. The pre-cone angle β_0 of the rotor has been assumed to be zero.

4. Results and discussion

We assume a symmetric NACA 0012 section to study both the cases. The influence of the relevant parameters for individual cases are discussed in the following subsections. The aerodynamic loads are computed by the Onera dynamic stall model. The coefficients of the Onera model s_z, k_{vz}, λ_z, α_z, a_{oz}, σ_z, d, w and e are given by Dunn and Dugundji (1992) for two Re ranges: $\mathrm{Re} > 3.4\times10^5$ and $\mathrm{Re} < 3.4\times10^5$. In this study, we assume $\mathrm{Re} > 10^6$ and choose the appropriate parameters. The elastic axis is chosen at the quarter-chord point. For both the models, structural damping has been

neglected. Though the effect of structural damping could be significant in any dynamical system, for the stall flutter case previous work suggests that the influence aerodynamic damping is more important than that of structural damping (Fragiskatos, 1999).

The differential equations of the Onera model are combined with the governing equations of the structural system. The resulting system of equations is solved in the time domain using a fourth-order variable-step Runge–Kutta integration scheme. At each time level the technique uses internal time step sizes smaller than the user-prescribed value till convergence is obtained. The nondimensional time step size chosen here is 0.01, based on the frequency of oscillation. The time step size conforms with the convergence criteria as well.

4.1. Single-degree-of-freedom pitching oscillation problem

Fragiskatos (1999) reports a parametric study on a pitching stall flutter model. However, the effect of structural nonlinearity, which could play a significant role on the stability and dynamical behavior of the system has not been considered. The influence of initial conditions on the bifurcation routes has not been reported either. These issues are addressed in the present work. The equation of motion for this case is given in Eq. (5) in a nondimensional form. We consider both self-excited and forced analysis of the system. System parameters are varied in the range of practical interest (Fragiskatos, 1999).

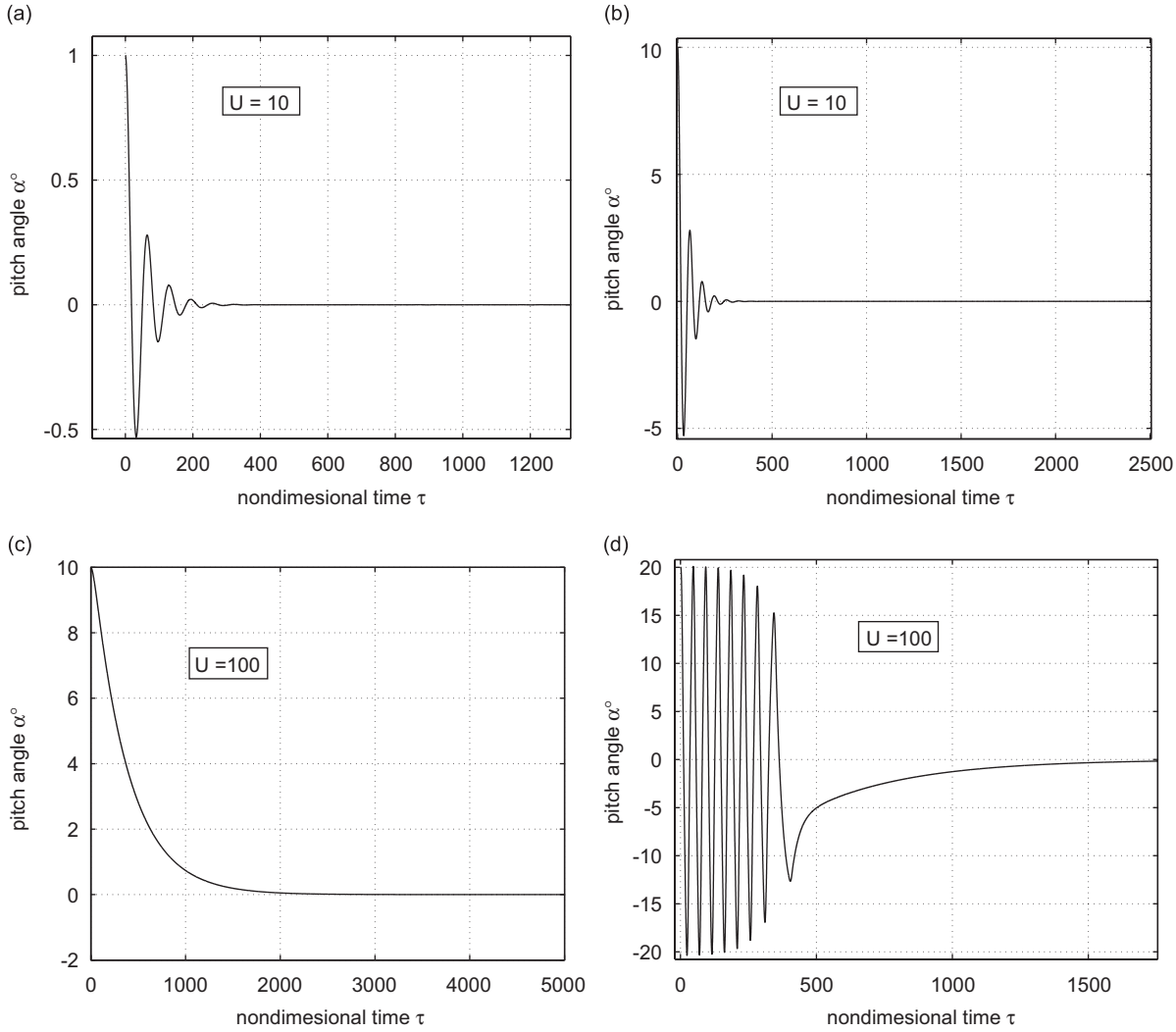

Fig. 2. Damped oscillation, $\alpha_m = 0.0$, with different initial conditions: (a) ICS 1°; (b) ICS 10°; (c) ICS 10°; (d) ICS 20°.

4.1.1. Self-excited system: effect of mean angle of attack, geometric nonlinearity

To study the self-excited system, the external moment at the right-hand side of Eq. (5) is assumed to be zero. The structural parameters are assumed to be $\mu = 100$, $r_\alpha = 0.5$ (Price and Fragiskatos, 2000). These values are kept constant throughout the simulations. In the unforced system, the nondimensional velocity U is the most important bifurcation parameter. Other relevant parameters are the mean angle of attack, structural nonlinearity and initial conditions. The single-degree-of-freedom pitching system shows a damped oscillation till the stall angle of the airfoil is reached. A nonzero mean angle or the structural equilibrium point (Fragiskatos, 1999), about which the initial perturbation is given, helps increase the airfoil angle of attack as U increases. However, with a zero mean angle, even a large U does not show the same. Some typical cases are presented in Fig. 2 with different initial perturbations. All cases are with zero mean angle of attack. The results for $U = 10$ are shown in Fig. 2(a),(b), and for $U = 100$ in Fig. 2(c),(d). Initial perturbations are evident in the plots as the starting point. In all the cases, the response always comes back to a damped oscillation.

A nonzero mean angle of attack changes the system behavior significantly. A static moment is applied in order to maintain a structural equilibrium position of nonzero mean angle of attack. The nondimensional velocity U is

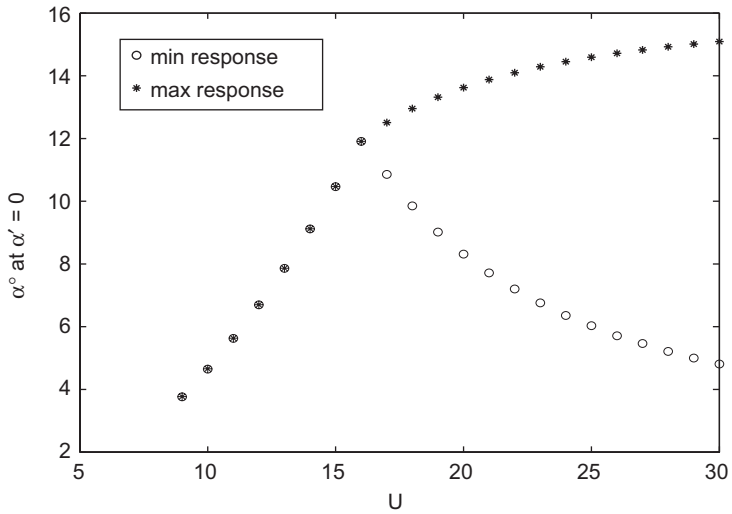

Fig. 3. Bifurcation plot for $\alpha_m = 4^\circ$, $\alpha_{\text{init}} = 10^\circ$.

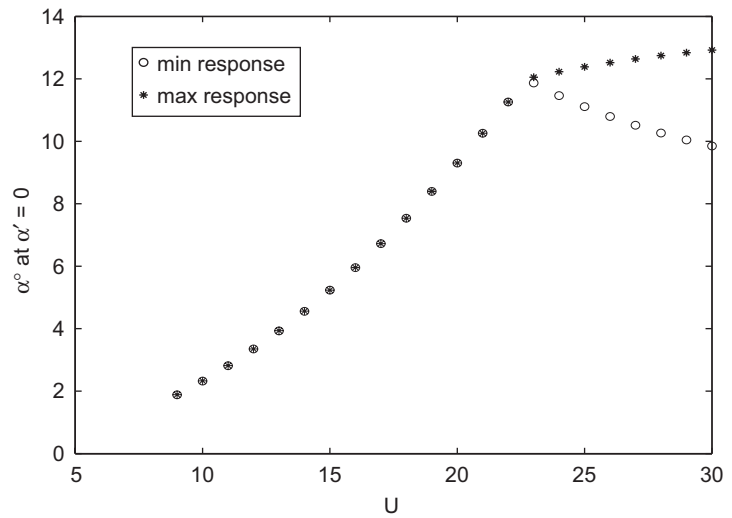

Fig. 4. Bifurcation plot for $\alpha_m = 2^\circ$, $\alpha_{\text{init}} = 10^\circ$.

considered as a bifurcation parameter. We consider a static equilibrium position around 4°. The resulting response is plotted in Fig. 3 for different U. The ordinate gives the pitch response at its maximum and minimum points, that is, where the derivative of the response (α') is zero. The initial condition for α is kept constant at 10°. As the figure shows, the response changes qualitatively after $U = 16$; it becomes oscillatory from a damped response. Therefore, $U = 16$ is the critical point or, the onset of stall flutter where limit cycle oscillation (LCO) starts.

Next, we consider a mean angle of 2°. The critical U at which LCO is obtained is 22 as shown in Fig. 4. Comparing this with the case of 4° mean angle of attack, we surmise that a smaller initial α_m takes a higher U to reach the LCO. It is also apparent from the above study that, as U increases, the mean angle of incidence α_m about which the oscillation occurs or dies down, increases. The LCO occurs only when α_m reaches past the stall angle, at a critical value of U (U_{cr}). A critical speed versus mean angle of attack study has been done in the mean angle of attack range of $1-10°$. The result is plotted in Fig. 5.

Next, we add structural nonlinearity to the system. A cubic stiffness is considered, as previously stated in Section 3. A cubic nonlinear term of $0.05\alpha^3$ is considered to that effect. In this case, the LCO occurs at $U = 28$, much beyond the previous case. The response is plotted in Fig. 6. It seems, adding cubic structural nonlinearity makes the U_{cr} value much

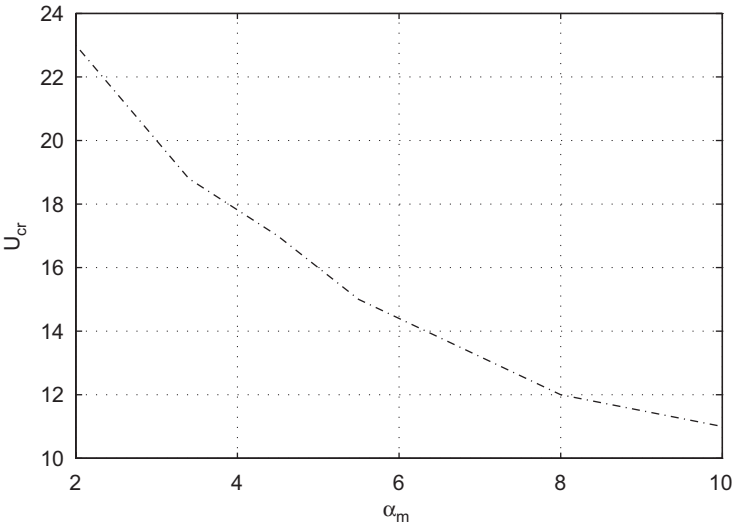

Fig. 5. Stall flutter boundary, U_{cr} versus α_m.

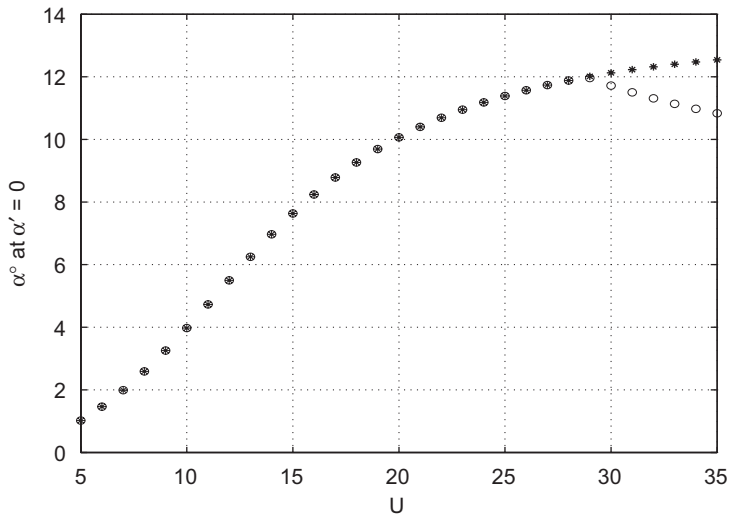

Fig. 6. Bifurcation plot for $\alpha_m = 4°$ and with cubic nonlinearity $\bar{K}_{\mathrm{nl}} = 0.05\alpha^3$, $\alpha_{\mathrm{init}} = 10°$.

higher. However, this effect could be due to the extra stiffness added to the system and not necessarily due to the nonlinearity.

4.1.2. Self-excited system: influence of initial conditions

By changing the initial condition of the self-excited system, different periodic attractors have been observed. When the initial perturbation is increased to 20°, the response pattern changes qualitatively. We observe a series of period-doubling flip bifurcations leading to an aperiodic response. We present the results for a mean angle of 0.5°. A single periodic response goes to period-2 at around $U = 6$ which leads to an aperiodic response at $U = 9.7$, after following a series of period-doubling bifurcations. The single periodic response is shown in Fig. 7 for $U = 5$ with the time history, phase plot and the frequency content. The period-2 response is presented in Fig. 8 for $U = 7$. After another flip bifurcation, a period-4 response occurs and it is shown in Fig. 9 for $U = 9.4$ in the same manner. Finally at $U = 9.7$, an aperiodic response is obtained. The time history is shown in Fig. 10(a). The phase plot in Fig. 10(b) does not look like a strange attractor; instead it resembles a quasiperiodic pattern. The frequency content shown in Fig. 10(c) reveals two peaks: 0.11 and 0.17 which are incommensurate. We have also taken Poincaré sections of the response and the Poincaré plot reveals a closed loop (not shown here), also indicating a quasiperiodic response. It should be noted that the natural frequency of the system (without the aerodynamic moment) is in the form of $1/U$. However, U itself acts as a bifurcation parameter to bring in this qualitative change. The frequencies of the response are seen in the Figs. 7–9(c).

When a mean angle of attack around 5.5° is chosen, again a similar quasiperiodic route is observed. However, the quasiperiodic response is obtained at a much lower U value and with a higher angular perturbation of 25°. For this case, a LCO appears around $U = 3$; period-doubling is observed at $U = 4$, and at $U = 5.1$ a quasiperiodic response similar

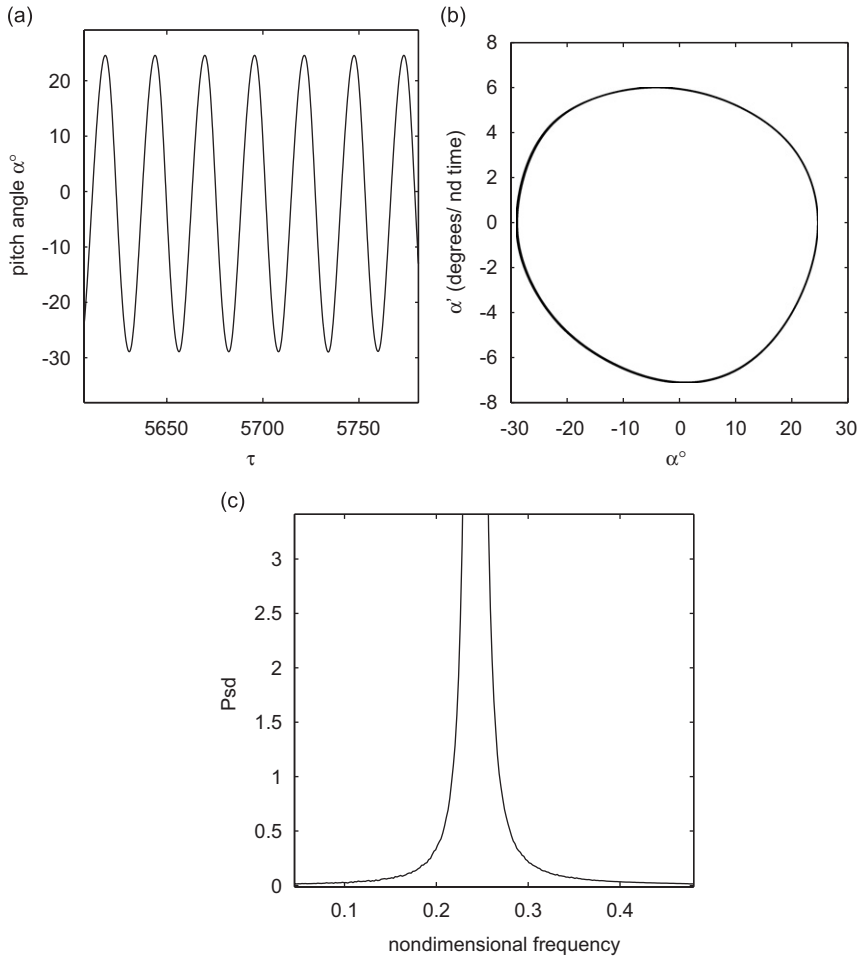

Fig. 7. For $\alpha_m = 0.5$, $\alpha_{\text{init}} = 20°$ and $U = 5$, period-1 response.

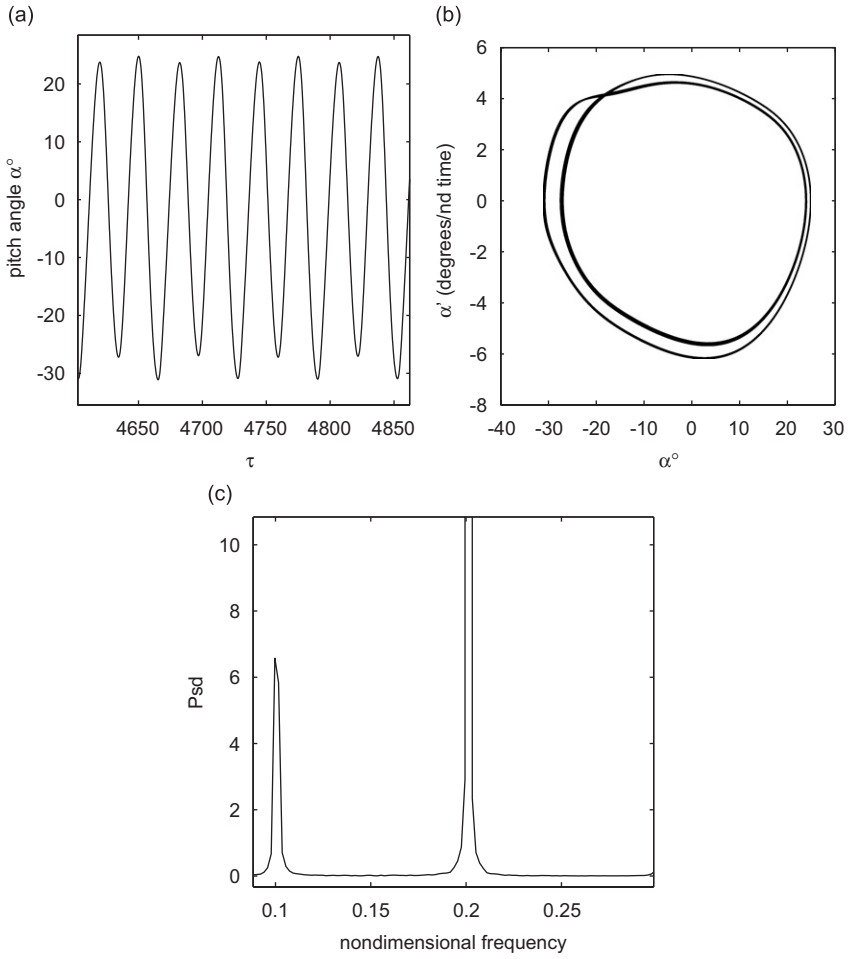

Fig. 8. For $\alpha_m = 0.5$, $\alpha_{\text{init}} = 20^\circ$ and $U = 7$, period-2 response.

to the previous case is obtained. Though we obtain identical paths to a quasiperiodic orbit for both cases, they occur at different U values: for a higher mean angle, LCO and quasiperiodic response occur at lower U. Also, the initial perturbation of α required to obtain a LCO and subsequent quasiperiodic attractor is higher for the higher mean angle of attack case. The bifurcation pattern with routes to quasi-periodicity is presented in Fig. 11 for $\alpha_m = 0.5^\circ$ case.

Cubic nonlinearity when added to the system modifies the bifurcation pattern, as shown in Fig. 12. A cubic spring stiffness of 0.01 slightly defers the quasiperiodic response to around $U = 10.1$ from 9.7 of the earlier case. However, a higher cubic stiffness of 0.1 significantly modifies the response, as shown in Fig. 13. In this case, a period-2 response, appears at U around 9 and no further period-doubling is obtained for U up to 30.

4.1.3. Forced oscillation

In this case, an external forcing term at the right-hand side of Eq. (5) is introduced in the form of harmonic forcing couple: $F_0 \sin(k_1\tau)$. We first assume $F_0 = 0.001$, $U = 10$, $k_1 = 0.2$ with a mean angle of attack of 5°. The solution is periodic. As F_0 is increased till 0.002 at an interval of 0.0005, we consistently obtain single periodic response throughout the range. This is shown in Fig. 14. It can also be observed that the amplitude of the period-1 response increases as the forcing amplitude increases. When U is changed to 15 and F_0 to 0.002, the response changes to an aperiodic one. The attractor in the phase plane is shown in Fig. 15, which resembles a chaotic attractor. Poincaré sections of the response are taken and the Poincaré points are plotted in Fig. 16. In this case, the entire phase plane looks populated by the Poincaré points, a signature of chaotic response. The frequency content plot in Fig. 17 shows many peaks which is observed in a chaotic pattern. The Lyapunov exponents are not computed, but a check with slightly different initial conditions has been done. We have considered two time histories with initial conditions different from each other by

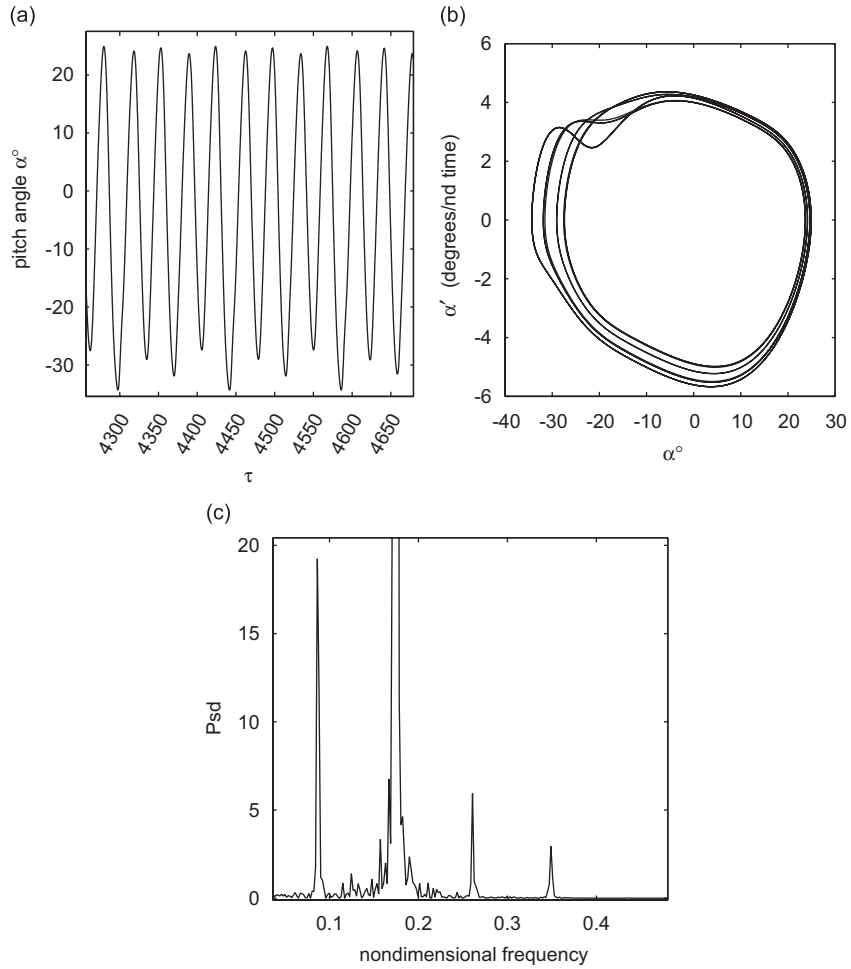

Fig. 9. For $\alpha_m = 0.5$, $\alpha_{\text{init}} = 20^\circ$ and $U = 9.4$, period-4 response.

10^{-3} radians and after a nondimensional time window of 1200, the time histories look significantly drifted from each other. This confirms the response to be chaotic. The two time histories are presented in Fig. 18. The separation of time histories from each other grows with time giving a rough approximation of a positive Lyapunov exponent (Fragiskatos, 1999; Wolf et al., 1985), which is a signature of chaos. Next, we follow the chaotic path backward by decreasing F_0 and the bifurcation plot is presented in Fig. 19. There are chaotic bands in between and the system uses period-doubling routes to chaos.

Next, the oscillation frequency k_1 is varied between 0.2 and 0.4 with an interval of 0.001. The bifurcation diagram presented in Fig. 20, shows an interesting behavior: a period-3 response. The response starts with chaos and remains so at the lower values of k_1. As k_1 increases to 0.22, a period-2 response is visible which becomes chaotic through a period-doubling cascade at $k_1 = 0.286$. At $k_1 = 0.295$, the chaotic response gives way to a period-3 response. The response remains so for the rest of the k_1 range.

4.2. Two-degree-of-freedom flap–edgewise oscillation

The combined flap and edgewise oscillation case has not received much attention in the nonlinear aeroelastic community. However, as mentioned earlier, such oscillations could potentially lead to structural damage. Chaviaropoulos (1999) and Chaviaropoulos et al. (2003) have presented a linear stability analysis along with the time domain results for a self-excited system. However, only a few cases with different nondimensional rotor speeds were studied. A quasi-steady Onera model was used for the linear stability analysis, and time domain results were simulated using grid based viscous flow solvers. Effects of external forcing and structural nonlinearity were not

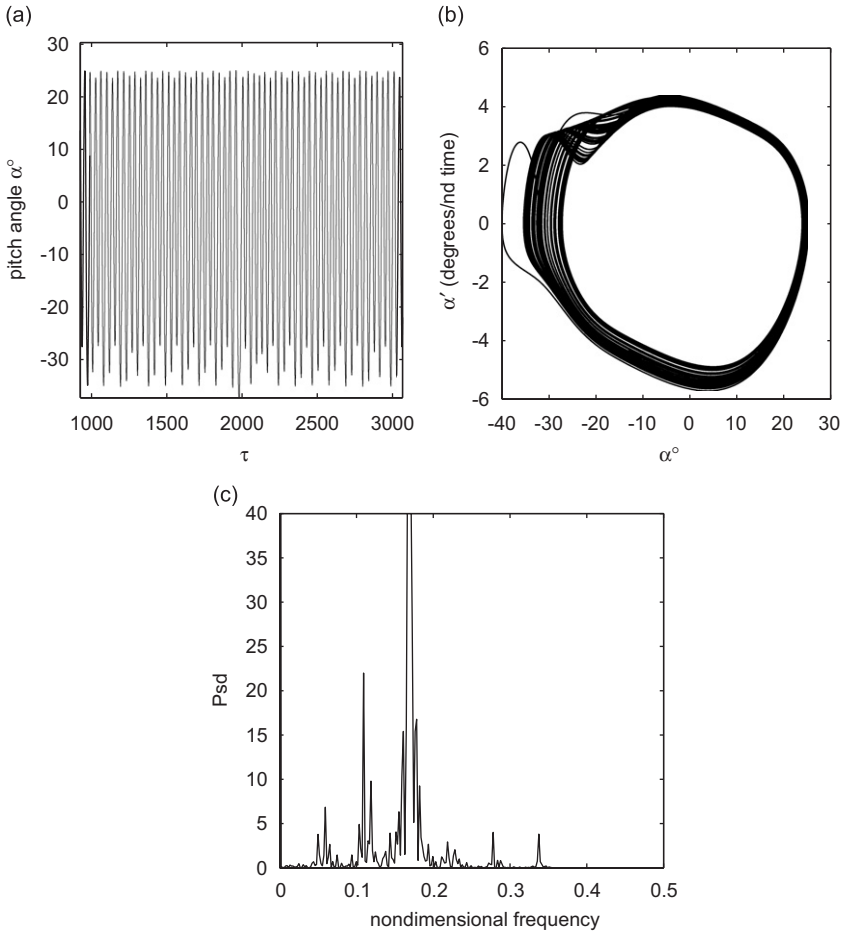

Fig. 10. For $\alpha_m = 0.5$, $\alpha_{\text{init}} = 20^\circ$ and $U = 9.7$, quasiperiodic response.

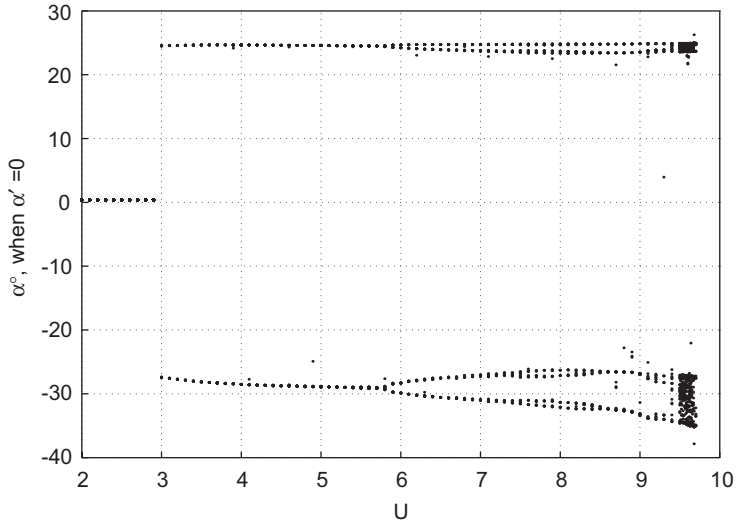

Fig. 11. Bifurcation plot, $\alpha_m = 0.5^\circ$, $\alpha_{\text{init}} = 20^\circ$, $K_{\text{nl}} = 0$.

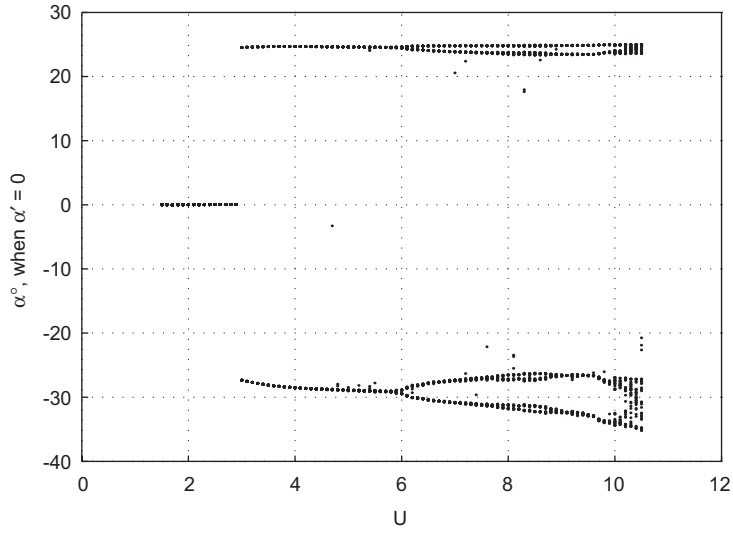

Fig. 12. Bifurcation plot, $\alpha_m = 0.5^\circ$, $\alpha_{\text{init}} = 20^\circ$, $K_{\text{nl}} = 0.01\alpha^3$.

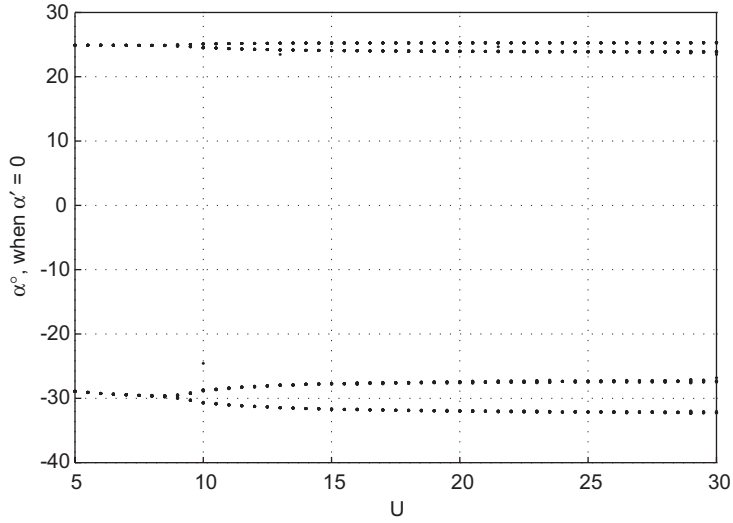

Fig. 13. Bifurcation plot, $\alpha_m = 0.5^\circ$, $\alpha_{\text{init}} = 20^\circ$, $K_{\text{nl}} = 0.1\alpha^3$.

investigated. The present study also considers parameters like structural stiffness for their influence on the system dynamical behavior. Effects of initial conditions have also been investigated which is done here. Geometric structural nonlinearity has been included in the model and its effect on the response studied. Finally, a forced response analysis is presented. Nondimensional amplitude and frequency of forcing have been varied as bifurcation parameters. The system shows super-harmonic and quasi-harmonic behavior at different forcing frequencies. No chaotic route has been found.

4.2.1. Verification with previous work

The equation of motion is given in the nondimensional form in Eq. (7); we assume, $1/\pi\mu = 0.02$ and pitch angle $\theta = 18^\circ$ which is above the stall angle of attack of the airfoil. These values are kept constant throughout the simulations. The structural stiffness values are, $\bar{\omega}_y = 7$, $\bar{\omega}_z = 4$. The Reynolds number is assumed to be $\text{Re} > 10^6$, with incompressible flow assumptions. External forcing is zero. For the same system, Chaviaropoulos et al. (2003) presented

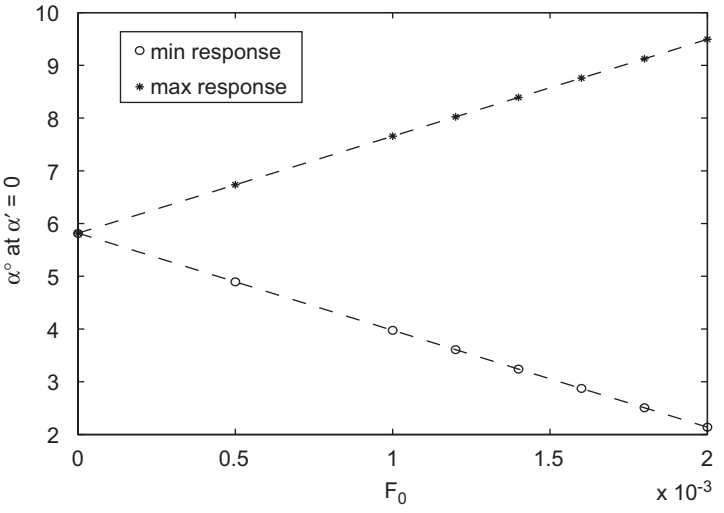

Fig. 14. F_0 as a bifurcation parameter, $U = 10$, $k_1 = 0.2$, $\alpha_m = 5.5^\circ$.

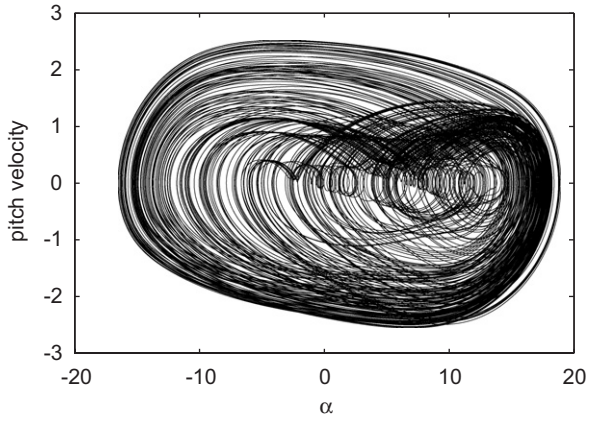

Fig. 15. Chaotic attractor at $U = 15$, $F_0 = 0.002$, $k_1 = 0.2$, $\alpha_m = 5.5^\circ$.

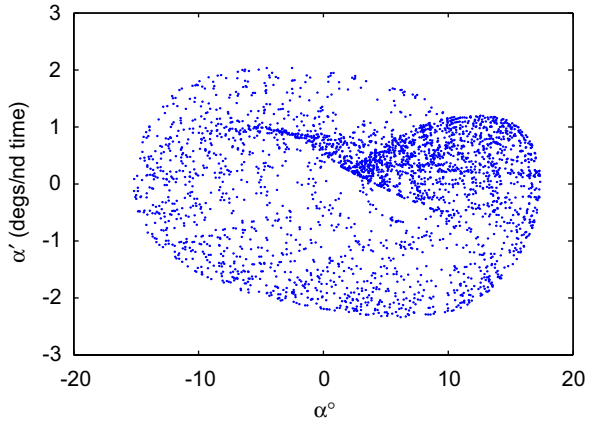

Fig. 16. Poincaré section plot for $U = 15$, $F_0 = 0.002$, $k_1 = 0.2$, $\alpha_m = 5.5^\circ$.

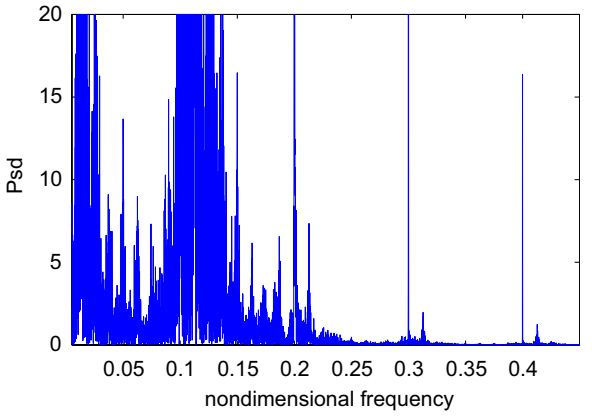

Fig. 17. Frequency content, $U = 15$, $F_0 = 0.002$, $k_1 = 0.2$, $\alpha_m = 5.5^\circ$.

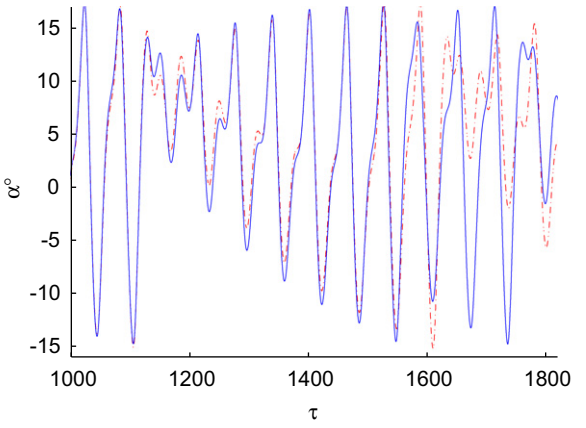

Fig. 18. Time histories with two initial conditions separated by $1e^{-3}$ radians, $U = 15$, $F_0 = 0.002$, $k_1 = 0.2$, $\alpha_m = 5.5^\circ$.

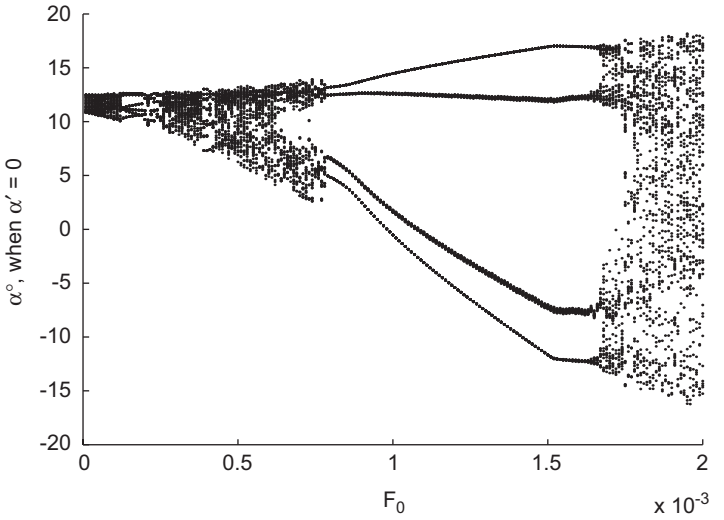

Fig. 19. F_0 as a bifurcation parameter, $U = 15$, $k_1 = 0.2$, $\alpha_m = 5.5^\circ$.

time domain results obtained by using a Navier–Stokes solver. The time domain solutions were accompanied by a linear stability analysis performed using quasi-steady Onera dynamic stall model. We start with comparing our time domain solutions with those presented by Chaviaropoulos et al. (2003). Two test cases with $k = 0.05$ and 0.1 are chosen, with zero initial conditions. For $k = 0.1$, a stable damped response is predicted by the Onera model, as was also reported by Chaviaropoulos et al. (2003). The time history of the response is given in Fig. 21 for both edgewise and flapwise oscillations. Both are aeroelastically stable. The flapwise oscillation matches almost perfectly with that reported by Chaviaropoulos et al. (2003). However, the edgewise oscillation shows a slightly higher amplitude than our result. Note that the results are compared for an initial time frame of (0–100), and a difference in the amplitude refers to a difference in the level of damping. We attribute this to numerical damping, which is likely to vary from one numerical model to another. The order of the edgewise response being very small (in the order of 10^{-3}), even a small amount of numerical damping could effectively change the order of the solution. A second test case with $k = 0.05$ and zero initial conditions, shows an unstable response, shown in Fig. 22. For this case, an unstable response was also reported by Chaviaropoulos et al. (2003) as well. However, they did not present any time history for this case.

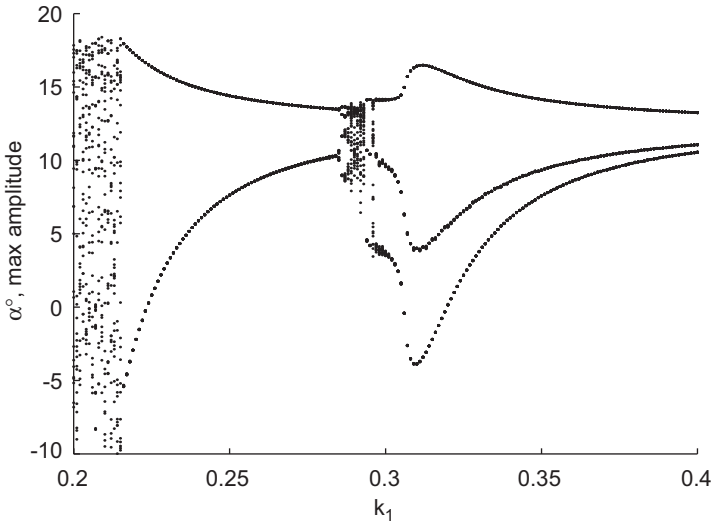

Fig. 20. k_1 as a bifurcation parameter, $U = 15$, $F_0 = 0.002$, $\alpha_m = 5.5^\circ$.

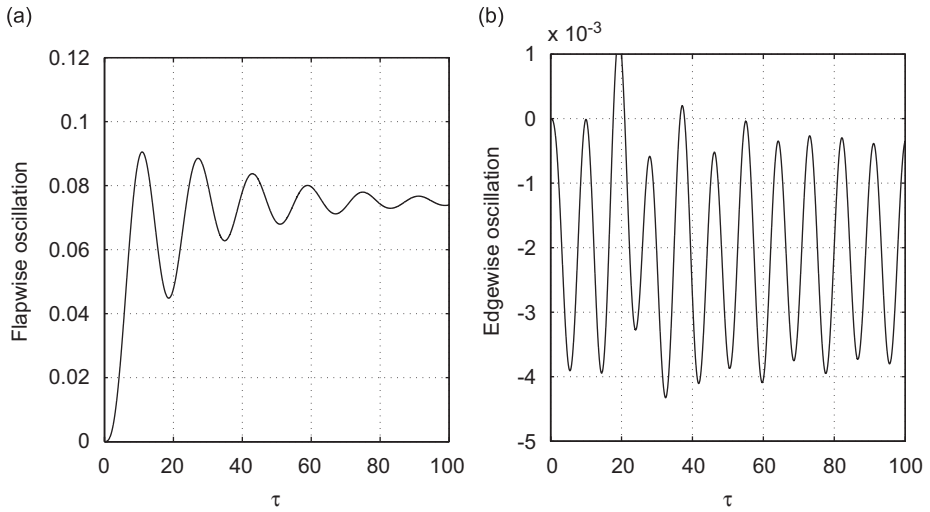

Fig. 21. Stable solution for flap–edgewise oscillation case for $k = 0.1$, $1/\pi\mu = 0.02$, $\bar{\omega}_y = 7$, $\bar{\omega}_z = 4$.

4.2.2. Self-excited system: effect of initial conditions and structural stiffness

As seen in the previous section, the system response is unstable at $k = 0.05$, further investigation shows that at higher values, only stable period-1 solutions are obtained. However, we observe that adding a nonzero initial condition could change this. This is shown in Fig. 23 for $k = 0.06$. With an initial perturbation of 0.5 in the flapping direction the response becomes unstable. Next we study the influence of structural stiffness in the flap and edgewise directions and their ratio as well. It is observed that rather than the ratio of $\bar{\omega}_z/\bar{\omega}_y$, individual values are more important. If we double both the stiffness, both flap and edgewise response decrease and no nonlinear effects are observed. This is presented in Fig. 24. Increasing the edgewise stiffness further while keeping the other fixed, the response in the edgewise direction alone is reduced, as shown in Fig. 25. We also consider a reduced stiffness in order to investigate the effect of higher flexibilities. For that, $\bar{\omega}_z$ is decreased gradually from the earlier value of 4. As a result, the earlier damped response undergoes a qualitative change and becomes periodic and then higher periodic. We present a typical case in Fig. 26, when $\bar{\omega}_z = 2$. The response shows a period-3 attractor; the phase plot has three loops. Thus, nonlinear behavior is introduced into the system with increased flexibility.

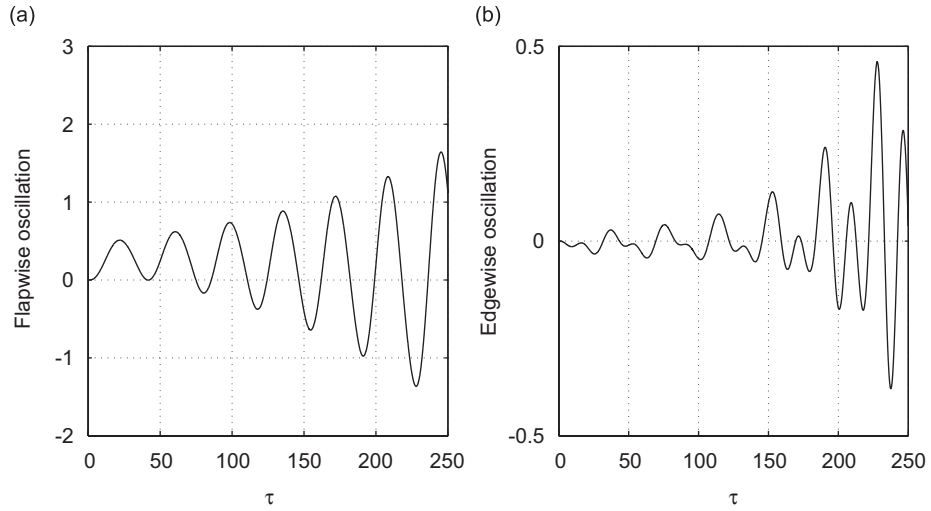

Fig. 22. Unstable solution for flap–edgewise oscillation case for $k = 0.05$, $1/\pi\mu = 0.02$, $\bar{\omega}_y = 7$, $\bar{\omega}_z = 4$.

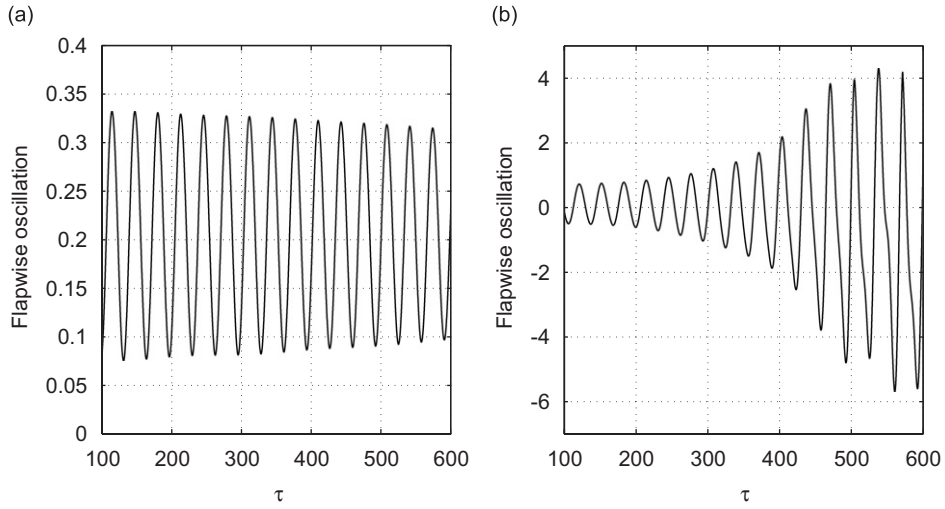

Fig. 23. Flapwise oscillation, for $k = 0.06$, $1/\pi\mu = 0.02$, $\bar{\omega}_y = 7$, $\bar{\omega}_z = 4$: (a) zero initial perturbation, (b) initial perturbation of 0.5 in flap.

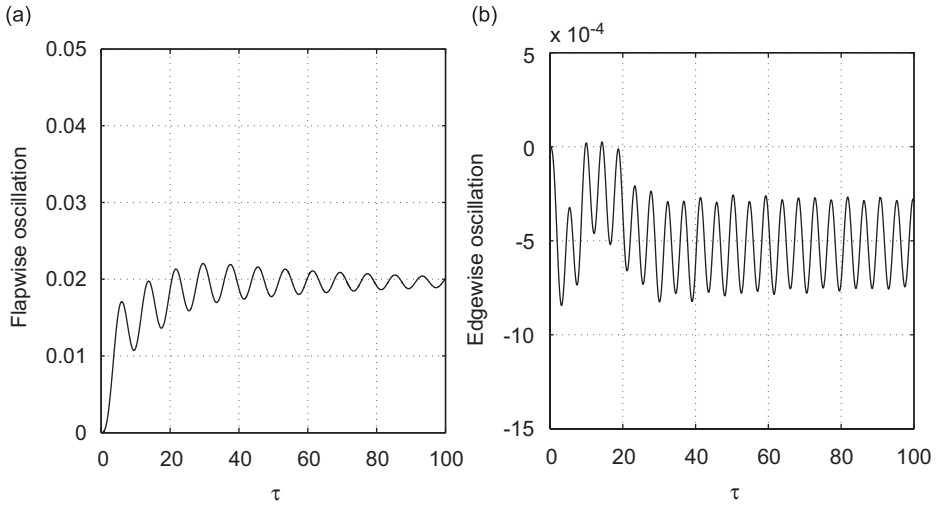

Fig. 24. Effect of structural stiffness, for $k = 0.1$, $1/\pi\mu = 0.02$, $\bar{\omega}_y = 7 \times 2$, $\bar{\omega}_z = 4 \times 2$: (a) flapwise oscillation, (b) edgewise oscillation.

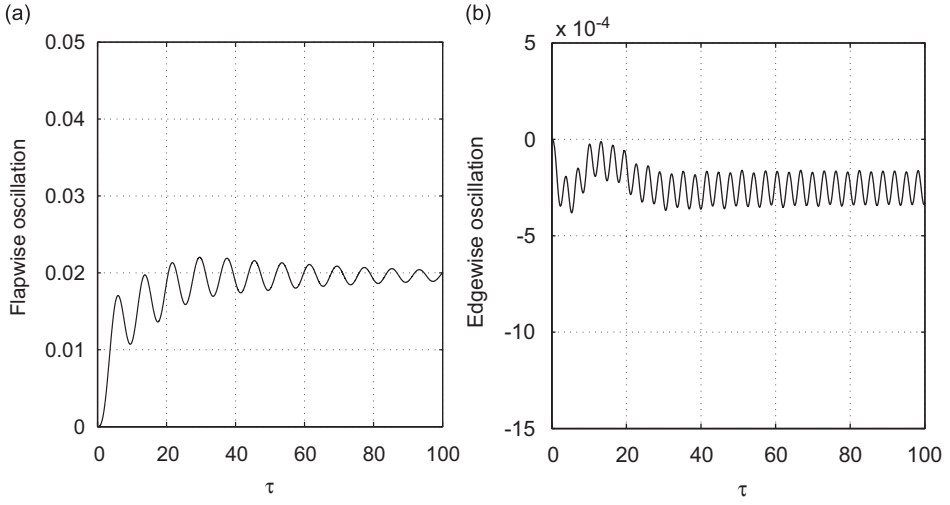

Fig. 25. Effect of structural stiffness, for $k = 0.1$, $1/\pi\mu = 0.02$, $\bar{\omega}_y = 20$, $\bar{\omega}_z = 4 \times 2$: (a) flapwise oscillation, (b) edgewise oscillation.

Finally a cubic nonlinearity in the flapwise direction is added. The flapwise direction is chosen because, oscillation amplitude in this direction is much larger than in the other; so it is expected that the effect of geometric nonlinearity will be more pronounced. However, no nonlinear dynamical behavior in the overall response has been observed. The effect of adding the cubic stiffness term has been similar to adding extra stiffness to the system, the resulting amplitude being smaller.

4.2.3. Forced oscillation

In the results presented above, the self-excited system has shown instabilities at low k. So far, no significant nonlinear dynamical behavior has been observed. To investigate the system dynamics further, we now add external forcing to it. A sinusoidal forcing term as shown in Eq. (7) is added to the system. In the previous system, we saw chaotic response appearing in the otherwise damped response after adding forcing. We once again vary the forcing amplitude ($\bar{F}_0$) and the nondimensional frequency of the forcing (k_1). Other parameters are kept at $\bar{\omega}_y = 7$, $\bar{\omega}_z = 4$, $k = 0.1$. Fig. 27 shows the bifurcation diagram of the response for forcing amplitude ($\bar{F}_0$) 0.0–0.002. Unlike the previous case, the maximum response at each cycle of oscillation is presented here. We observe only period-1 oscillations in this range. However, the

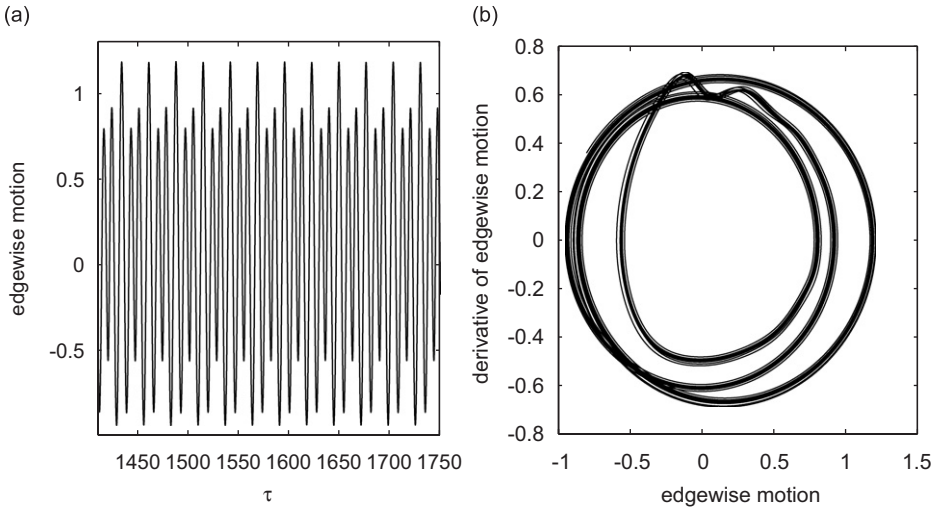

Fig. 26. Effect of structural stiffness, for $k = 0.1$, $1/\pi\mu = 0.02$, $\bar{\omega}_y = 7$, $\bar{\omega}_z = 4/2$: (a) flapwise oscillation, (b) edgewise oscillation.

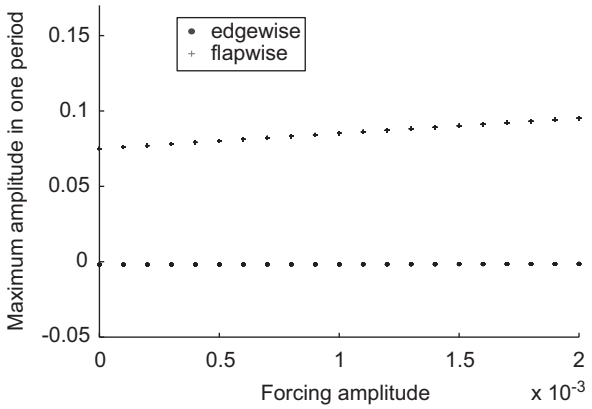

Fig. 27. F_0 as a bifurcation parameter, $k_1 = 0.2$.

amplitude of response increases with the amplitude of forcing. On the other hand, variation of nondimensional frequency k_1 shows interesting dynamical behavior. The system shows the presence of two frequencies: one is the forcing frequency of oscillation and the other is the frequency of the unforced system. The nondimensional frequency of oscillation of the unforced system is found to be 0.7. At lower k_1 values, the influence of the unforced natural frequency is stronger. When k_1 is 0.05, fourteenth-order harmonics are observed. Similarly, seventh-order harmonics are present for $k_1 = 0.1$. For $k_1 = 0.15$, the frequencies are incommensurate so quasiperiodic response is observed. However, as k_1 increases further, the presence of higher-harmonics and quasi-harmonics is not apparent from the time histories and phase plots of the response; though an FFT analysis continues to show a rather weak presence of frequency 0.7.

The time history and frequency content plot for $k_1 = 0.05$ is shown in Fig. 28. The response shows two main frequencies, 0.05 and 0.7, that is, higher harmonic of fourteenth-order is present. Similarly, for $k_1 = 0.1$, the frequency content confirms (Fig. 29(b)), the presence of seventh-order harmonics in the response. The next case with $k_1 = 0.15$, is presented in Fig. 30. The frequencies present are 0.15 and 0.7 which are incommensurate, hence indicating a quasiperiodic behavior. As the reduced forcing frequency k_1 is increased further, the response gradually shows stronger influence of k_1 alone. The time history for $k_1 = 0.2$ is shown in Fig. 31(a), where the presence of a higher harmonic is not visible. The frequency content of this response, shown in Fig. 31(b), shows a strong peak around 0.2. Though an extremely weak presence of frequency 0.7 is also observed, this is not reflected on the time history of the response.

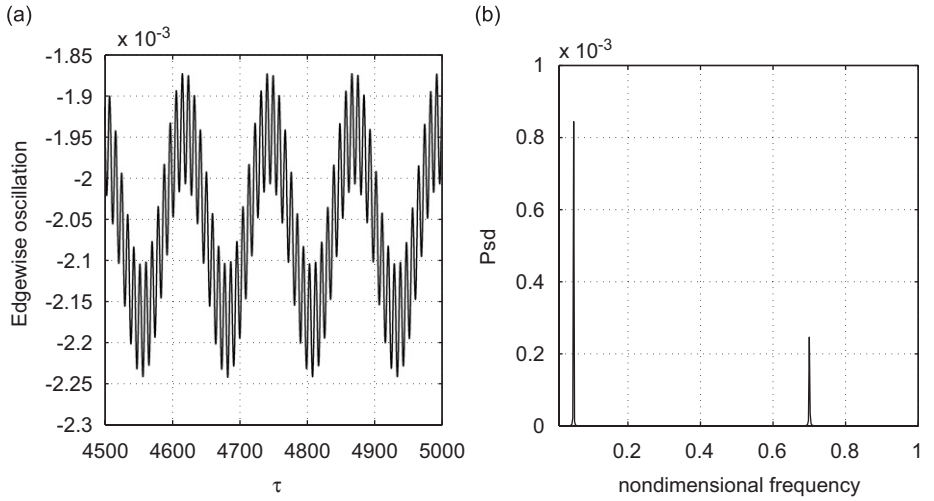

Fig. 28. Forced response, $k = 0.1$, $k_1 = 0.05$, $F_0 = 0.001$, $\bar{\omega}_y = 7$, $\bar{\omega}_z = 4$. Higher-harmonic response: (a) edgewise oscillation time history, (b) edgewise oscillation frequency content.

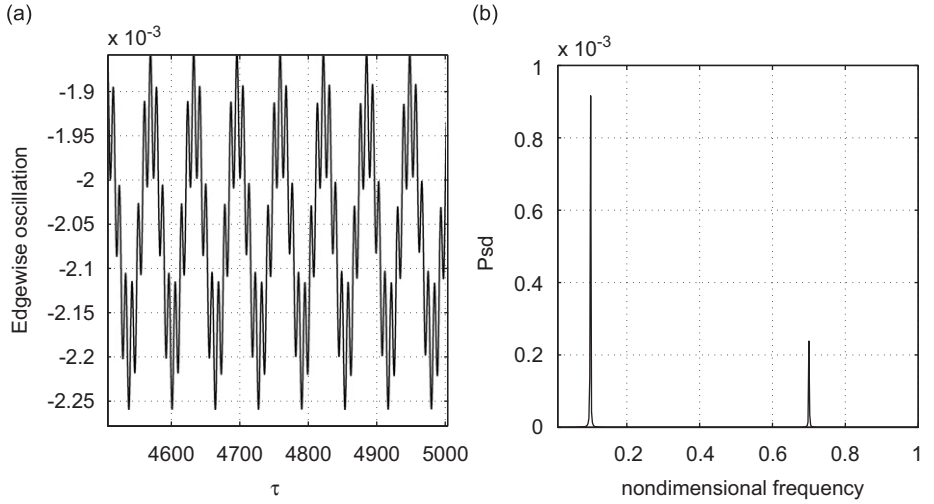

Fig. 29. Forced response, $k = 0.1$, $k_1 = 0.1$, $F_0 = 0.001$, $\bar{\omega}_y = 7$, $\bar{\omega}_z = 4$. Higher-harmonic response: (a) edgewise oscillation time history, (b) edgewise oscillation frequency content.

5. Conclusions

A nonlinear aeroelastic analysis of a two-dimensional airfoil is presented here during stall-induced oscillations. The focus has been to investigate the influence of various system parameters on the aeroelastic stability and nonlinear dynamical response. Emphasis is given on parameters like structural nonlinearity and initial conditions. Two different stall oscillation models are considered: pitching oscillation and flap–edgewise oscillation. Both self-excited as well as forced oscillations are studied. An engineering stall model by Onera is used to calculate the aerodynamic loads in the dynamic stall regime. This model is well established and is based on steady and unsteady experimental data. Coefficients of the Onera model are taken from available data in the literature.

The analysis is performed with parametric variations and the resulting bifurcation behavior is noted. The first system shows the presence of a strong nonlinear behavior even without structural nonlinearity and external forcing. For

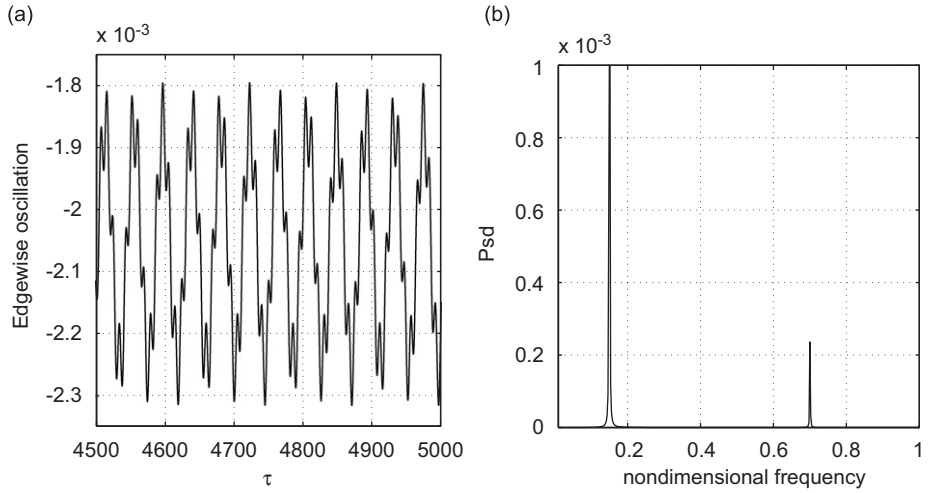

Fig. 30. Forced response, $k = 0.1$, $k_1 = 0.15$, $F_0 = 0.001$, $\bar{\omega}_y = 7$, $\bar{\omega}_z = 4$. Quasi-harmonic response: (a) edgewise oscillation time history, (b) edgewise oscillation frequency content.

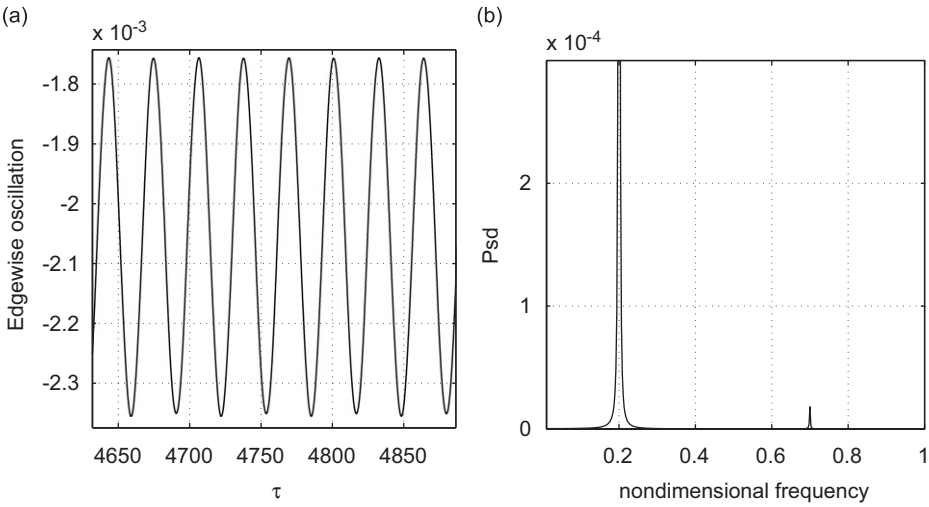

Fig. 31. Forced response, $k = 0.1$, $k_1 = 0.2$, $F_0 = 0.001$, $\bar{\omega}_y = 7$, $\bar{\omega}_z = 4$. Predominantly harmonic response: (a) edgewise oscillation time history, (b) edgewise oscillation frequency content.

example, quasiperiodic attractors have been found in the self-excited system without structural nonlinearity. The bifurcation behavior is influenced by many parameters: mean angle of attack, initial conditions and structural nonlinearity. For the forced system, the bifurcation parameters are forcing frequency and amplitude. Forcing induces chaotic response in the otherwise damped system. Forcing amplitude as a bifurcation parameter shows chaotic routes through a series of period-doubling bifurcations. Forcing frequency shows the presence of period-3 attractors, culminating into chaos.

For the flap–edgewise oscillation case, not much work has been done before. We have chosen some test cases from previously published results and verified our results with those. We have varied system parameters like structural stiffness, initial conditions and structural nonlinearity. Initial conditions influence the stability behavior significantly. Structural stiffness in the flap and edgewise directions do not bring in significant qualitative changes in the response, except at low values. For the forced system, there are some interesting patterns as the forcing frequency is varied. Super-harmonic and quasiperiodic response are observed at lower values of the forcing frequency. However at higher values, the response becomes predominantly period-1.

References

Alighanbari, H., Price, S.J., 1996. The post hopf bifurcation response of an airfoil in incompressible, two-dimensional flow. Nonlinear Dynamics 10, 381–400.

Beedy, J., Barakos, G., Badcock, K.J., Richards, B.E., 2003. Nonlinear analysis of stall flutter based on the Onera aerodynamic model. The Aeronautical Journal 107, 495–509.

Chaviaropoulos, P.K., 1999. Flap/lead–lag aeroelastic stability of wind turbine blade sections. Wind Energy 2, 99–112.

Chaviaropoulos, P.K., Srensen, N.N., Hansen, M.O.L., Nikolaou, I.G., Aggelis, K., Johansen, J., Gaunaa, M., Hambraus, T., Geyr, H.F.v., Hirsch, C, Shun, K., Voutsinas, S., Tzabiras, G., Perivolaris, Y., Dyrmose, S.Z., 2003. Viscous and aeroelastic effects on wind turbine blades. The VISCEL project. Part II: aeroelastic stability investigations. Wind Energy 6, 387–403.

Dunn, P., Dugundji, J., 1992. Nonlinear stall flutter and divergence analysis of cantilevered graphite/epoxy wings. AIAA Journal 30, 153–162.

Fragiskatos, G., 1999. Nonlinear response and instabilities of a two-degree-of-freedom airfoil oscillating in dynamic stall. M.Eng. Masters Thesis, McGill University, Montreal, Canada.

Fung, Y.C., 1955. An Introduction to the Theory of Aeroelasticity. Wiley, New York.

Lee, B.H.K., Price, S.J., Wong, Y.S., 1999. Nonlinear aeroelastic analysis of airfoils: bifurcation and chaos. Progress in Aerospace Sciences 35, 205–334.

Leishman, J.G., Beddoes, T.S., 1989. A semi-empirical model for dynamic stall. Journal of the American Helicopter Society 34, 3–17.

Peters, D.A., 1985. Towards a unified lift model for use in rotor blade stability analyses. Journal of American Helicopter Society 30, 32–42.

Petersen, J.T., Madsen, H.A., Bjoerck, A., Enevoldsen, P., Øye, S., Ganander, H., Winkelaar, D., 1998. Prediction of dynamic loads and induced vibrations in stall. Risoe National Laboratory Risoe-R-1045(EN), pp. 1–160.

Price, S.J., Fragiskatos, G., 2000. Nonlinear aeroelastic response of a two-degree-of-freedom airfoil oscillating in dynamic stall. In: Ziada, S., Staubli, T. (Eds.), Proceedings of the Seventh International Conference on Flow Induced Vibration, Rotterdam, The Netherlands, pp. 437–444.

Tang, D.M., Dowell, E.H., 1993a. Comparison of theory and experiment for nonlinear flutter and stall response of a helicopter blade. Journal of Sound and Vibration 165, 251–276.

Tang, D.M., Dowell, E.H., 1993b. Nonlinear aeroelasticity in rotorcraft. Journal of Mathematical and Computer Modelling 18, 157–184.

Tran, C.T., Petot, T., 1981. Semi-empirical model for the dynamic stall of airfoils in view of the application to the calculation of responses of a helicopter blade in forward flight. Vertica 5, 35–53.

Wolf, A., Swift, B.J., Swinney, H.L., Vastano, J.A., 1985. Determining Lyapunov exponents from a time series. Physica D 16, 285–317.